Swelling and Dissolution Behavior of Poly(methyl methacrylate) Films in Methyl Ethyl Ketone/Methyl Alcohol Mixtures Studied by Optical Techniques

D. F. STAMATIALIS,[1,*] M. SANOPOULOU,[1] I. RAPTIS[2]

[1] Physical Chemistry Institute, Demokritos National Research Center, GR-15310 Aghia Paraskevi, Athens, Greece

[2] Institute of Microelectronics, Demokritos National Research Center, GR-15310 Aghia Paraskevi, Athens, Greece

Received 29 March 2001; accepted 12 June 2001

ABSTRACT: Swelling and dissolution behavior of poly(methyl methacrylate) (PMMA) films during unidimensional penetration of methyl ethyl ketone/methyl alcohol (MEK/MA) liquid mixtures at 22°C is presented. Optical microscopy and two-beam interferometry were applied to clamped PMMA films to obtain information on penetration kinetics and penetrant concentration profiles. Dissolution by pure MEK was initially controlled by Case II penetration kinetics and at later stages of the process, by stress cracking in the absence of a surface layer. Introduction of increasing amounts of MA in the liquid solvent resulted in moderation of the fragmentation process, enhanced penetration rates at the early stages of the process, deviations from Case II kinetics at the later stages, and the existence of a surface layer. These results indicate that penetration of MEK/MA mixtures and dissolution of PMMA are characterized by lower diffusion Deborah, and higher dissolution, numbers compared to those of pure MEK. Swelling by pure MA, as well as by nonsolvent MEK/MA mixtures, was characterized by Case II penetration kinetics. A pronounced minimum in the penetration rate versus liquid mixture composition plot was observed at 30 : 70 v/v MEK/MA composition. Laser interferometry was applied to very thin PMMA films, supported on a silicon substrate, to study selected cases. The results obtained were very similar to those obtained by optical microscopy. © 2002 John Wiley & Sons, Inc. J Appl Polym Sci 83: 2823–2834, 2002; DOI 10.1002/app.10258

Key words: dissolution of poly(methyl methacrylate); case II transport; two-beam interferometry; laser interferometry

INTRODUCTION

Penetration of a micromolecular species from a bulk liquid phase into an initially dry polymer film, driven by a chemical potential gradient, is normally accompanied by swelling and plasticization of the polymer. The penetrant may be a solvent or a nonsolvent of the particular polymer, depending on the thermodynamic properties of the polymer–penetrant pair. In the case of nonsolvents, penetration and swelling are the only steps of the sorption process and a uniform swollen polymer phase exists at the final equilibrium state. In the case of solvents, the swelling polymer eventually dissolves in the liquid solvent phase. Although both processes involve swelling of the initially dry polymer film, here the former case is

* *Present address:* European Membrane Institute Twente, University of Twente, Chemical Technology Department, PO Box 217, NL-7500 AE Enschede, The Netherlands.

Correspondence to: M. Sanopoulou (sanopoul@mail.demokritos.gr).

Contract grant sponsor: National Research Center Demokritos; contract grant number: 602.

Journal of Applied Polymer Science, Vol. 83, 2823–2834 (2002)

termed *swelling,* to be distinguished from the latter, termed *dissolution.*

Penetration kinetics in glassy polymer–organic penetrant systems exhibit a variety of deviations from diffusion-controlled (Fickian) kinetics. In liquid penetration experiments, in which a penetrant front B advancing into the polymer can be observed, a simple descriptive way to quantify deviations from Fickian kinetics is possible on the basis of the power law

$$X_B = kt^m \tag{1}$$

where X_B is the distance (in a suitable frame of reference) covered by the penetrant front B at time t, and k and m are constants. Under semi-infinite medium conditions, Fickian (Case I) kinetics is characterized by $m = 0.5$. Increasing values of m denote increasing deviations from Fickian kinetics, with $m = 1$ for Case II diffusion.

Non-Fickian kinetics is most commonly attributed to slow viscous molecular relaxations of the glassy polymer structure (in response to penetrant-induced osmotic stresses) that occur on time scales comparable to that of the diffusion process.[1–4] Non-Fickian behavior can be discussed in terms of a dimensionless parameter, the diffusion Deborah (DEB) number, defined as[5]

$$\text{DEB} = \tau_R/\theta$$

where τ_R is a characteristic relaxation time and θ is a characteristic diffusion time of the polymer–penetrant mixture. For the penetration experiments, in which the polymer substrate behaves throughout as a semi-infinite medium, θ is given by[6]

$$\theta = \frac{(X_{Bm})^2}{D}$$

where X_{Bm} is the maximum distance attained by front B in each experiment and D is the mutual diffusion coefficient in the appropriate frame of reference. In the systems under study, both D and τ_R are strong functions of the penetrant concentration. The DEB number may be used to define the conditions under which non-Fickian behavior is expected to occur. Thus at high concentrations and/or temperatures, where the polymer–penetrant mixture is well above T_g, molecular relaxation is much faster than diffusional transport and Fickian diffusion in the fully relaxed polymer is observed, characterized by DEB $\ll$ 1. At sufficiently low temperatures and/or concentrations, where the system is well within the glassy state and behaves purely elastically, Fickian kinetics is again observed, characterized by DEB $\gg$ 1. Deviations from Fickian kinetics are expected at intermediate values of DEB, where the system behaves viscoelastically. Under appropriate conditions[5,6] Case II transport may be observed, characterized by a sharp penetrant front separating nearly fully relaxed from unrelaxed polymer and advancing into the polymer linearly with time. In this case, diffusion of the penetrant in the swollen polymer phase is fast in relation to molecular relaxation at the sharp penetrant front (so that the penetration rate is relaxation-controlled) and the penetrant concentration behind the front is practically uniform. The concentration profile is also characterized by a low-concentration precursor front preceding the sharp front.[1,6]

As already noted, the normal dissolution process involves a third step besides penetration of the solvent and swelling of the polymer, that is, the disentanglement of the macromolecular chains from the swollen, plasticized polymer region followed by diffusion into the pure solvent phase. Ueberreiter[7] has divided the penetrated polymer region during dissolution into the following four layers arranged in the order of increasing penetrant concentration: (1) the infiltration layer, next to the pure polymer region; (2) the solid swollen layer; (3) the gel (rubberlike) layer; and (4) the liquid layer, next to the pure solvent. During dissolution of a glassy polymer all four layers are expected to exist and constitute what was termed by Ueberreiter[7] a "normal surface layer," the most extended part of which is the gel layer. Under semi-infinite medium conditions, the surface layer attains a constant thickness and the magnitude of the latter is determined by the relative rates of solvent penetration and polymer chain disentanglement. Furthermore, Ueberreiter[7] distinguished between the thermodynamic and kinetic suitability of a solvent. The kinetic suitability is determined by the molecular size and shape of the solvent and is mainly expressed in its high rate of penetration into the polymer matrix. The thermodynamic suitability is determined by the polymer–penetrant interactions. A thermodynamically good solvent facilitates the disentanglement of polymer chains by loosening up the structure; consequently, as the thermodynamic suitability of the solvent increases, the thickness of the surface layer decreases. More

recently, Peppas et al.[8] defined a dissolution number N_s as

$$N_s = \tau_d/\tau_p$$

where τ_d is a characteristic time for polymer disentanglement and τ_p is a characteristic time for solvent penetration. For cases of DEB $\gg$ 1 or DEB $\ll$ 1, where penetration is diffusion controlled, $\tau_p = \theta$, whereas for cases of DEB $\sim$ 1, where penetration is relaxation controlled, $\tau_p = \tau_R$. If $N_s > 1$ the polymer disentanglement rate is lower than the solvent penetration rate, resulting in a thick surface layer. If $N_s < 1$, the disentanglement rate is higher than the solvent penetration rate, yielding a thin surface layer.

When penetration of the solvent is relaxation controlled, dissolution may occur by stress-induced cracking. In this case the polymer structure responds to the penetrant-induced stresses by brittle failure. In the case of stress cracking, usually no surface layer is observed, indicating that the rate of relaxation is much lower than the rate of chain disentanglement ($N_s \ll 1$).

Swelling and dissolution of polymers are important phenomena in various applications, as for example in drug-delivery systems and microelectronics through lithographic processes.[8,9] The lithographic step of integrated circuit fabrication involves selective dissolution of the irradiated (positive resist) or of the nonirradiated (negative resists) areas of a polymeric resist. The developer often consists of a solvent/nonsolvent mixture, as for example in the case of poly(methyl methacrylate) (PMMA), which is used as a positive photoresist. Progress in the lithographic processes used in mass production seriously affects the miniaturization of semiconductor devices.[10,11] Therefore, an in-depth understanding of polymer dissolution and swelling is necessary. Fundamental studies on the transport and dissolution mechanisms in glassy polymer–pure penetrant liquid systems involve both extensive experimental and modeling work. Penetration and dissolution kinetics have been studied by a variety of techniques, such as optical microscopy,[7,12,13] refractometry,[7] laser interferometry,[10,14–16] ellipsometry,[17,18] critical angle illumination microscopy,[8] and fluorescence methods.[16] Penetrant concentration profiles have been obtained by interferometry,[7,12,13] MRI analysis,[19] fluorescence quenching,[10] Rutherford backscattering,[20] and optical microdensitometry.[12,21] The above-mentioned techniques were applied during transport of solvents[7,8,10,12,13,15–17,19] or nonsolvents[12–14,17,18,21] in free films,[7,21] films clamped between glass plates,[12,13] or, finally, in supported films.[8,10,14–20]

Some of these techniques have been applied to the study of swelling and dissolution behavior of polymer films by solvent/nonsolvent binary mixtures.[11,22–26] However, only a few studies have covered the full range of solvent/nonsolvent compositions (ranging from pure solvent to pure nonsolvent)[27,28] and, moreover, the recorded signal of the optical method applied is easily interpreted only in limiting cases of pure Case II or Fickian kinetic behavior. In this work we present a phenomenological study on the effect of the composition of a solvent/nonsolvent binary mixture on the swelling and dissolution behavior of PMMA films using methyl ethyl ketone (MEK) and methyl alcohol (MA) as solvent and nonsolvent, respectively. Optical microscopy and two-beam interferometry were applied to obtain detailed information on the kinetics of penetration and the concentration profiles during unidimensional penetration into, and swelling or dissolution of, clamped polymer films. The dissolution process was also studied in very thin supported films by laser interferometry (a technique that, although it provides less direct and detailed information on the dissolution process, corresponds more closely to the conditions of lithography), and the results of the two methods were compared.

EXPERIMENTAL

Materials

Commercial PMMA (Elvacite 2041) in the form of powder was supplied by Dupont (Toronto, Canada) with the following specifications: M_w = 405,000, M_n = 149,000, M_w/M_n = 2.45. MA, MEK, and methyl isobutyl ketone (MIBK) were of analytical reagent grade.

Film Preparation and Characterization

Films for Optical Microscopy and Two-Beam Interferometry

Films of thickness ℓ = 30–50 μm were prepared by casting an 11% w/w solution of PMMA (prefiltered though a G4 sintered glass filter) in MIBK on a clean glass surface with the aid of a knife blade moving on rails. After subsequent evaporation in an atmosphere partially saturated with

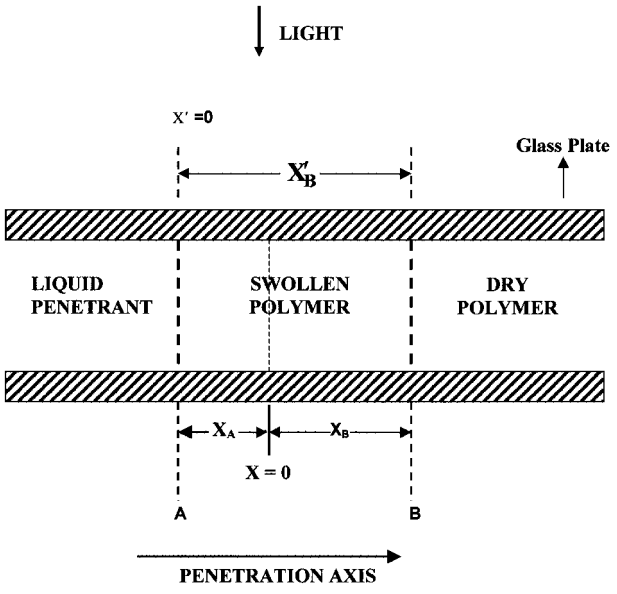

Figure 1 Schematic presentation of experimental setup for optical microscopy and two-beam interferometry measurements during liquid penetration in clamped PMMA films (see text).

MIBK vapor, the film was removed from the glass plate, evacuated for 10 days, and then heated gradually in an oven over a period of 24 h to 130°C and maintained at that temperature for 24 h. Then the temperature was gradually cooled down to 70°C, maintained at that temperature for 24 h, and then allowed to cool down to room temperature.

The T_g of the films, determined by DSC using a Dupont 910 instrument at a heating rate of 5°C/min, was found to be 114°C.

Films for Laser Interferometry

A solution of 8% w/w of PMMA in MIBK was spin coated on a silicon wafer at 4000 rpm for 30 s, and the films obtained were subjected to the same heating treatment as above. The thickness of the initially dry films, measured with a Talystep, were found to be 0.80–0.90 μm.

Methods

Optical Microscopy and Two-Beam Interferometry

The experimental setup is illustrated schematically in Figure 1. A 3×5 mm^2 rectangular polymer sample was sandwiched between two glass plates, held together by spring clips. The sandwiched film was immersed in a petri dish containing the liquid penetrant at room temperature (22 $\pm$ 1°C), and the whole assembly was placed on the stage of an Amplival Pol-U microscope (Jena, Germany). In this way, penetration across the film is prevented by the glass plates and can occur only along the film (Fig. 1). This technique allows *in situ* observation of the transport process under semi-infinite medium conditions,[12,13] by means of a light beam perpendicular to the direction of penetration. The penetrant front (B) advancing into the polymer (see Fig. 1) marks a sharp change in the penetrant concentration gradient and, consequently, in the corresponding refractive index gradient and is seen in the microscope as a black line. In the case of nonsolvents, the swelling edge (A) of the film, moving outward, is also visible. The positions of A and B at time t were recorded, in terms of the space coordinate X, using the position of the edge of the unswollen film at $t = 0$ as the origin. The relevant distances are represented by positive numbers X_A and X_B, respectively, whereas $X'_B = X_B + X_A$ represents the position of B, in terms of space coordinate X', using front A as origin (Fig. 1).

The microscope was also equipped with a two-beam interferometric device operating on the shearing principle.[12,13] A system of colored interference fringes, aligned in the direction of penetration X', is formed in the optical field. The fringe pattern could be recorded using an attached CCD camera, connected to a PC. The variation of the refractive index along X is reflected in lateral fringe displacements, which are proportional to the corresponding optical path differences (OPD). The fringe displacement at any location X', $\Delta y(X')$, within the penetrated film varies during the course of the experiment and, therefore, must be measured relative to a portion of the same fringe that remains fixed. The portion of the fringe that was located in the pure liquid was used for this purpose. Thus, the OPD profile, normalized with respect to the OPD of the dry polymer Δy_0, is given by

$$\frac{\Delta y(X')}{\Delta y_0} = \frac{n(X')\ell_X - n_1\ell_1}{n_2\ell_2 - n_1\ell_1} \qquad (2)$$

In eq. (2), n is the refractive index; the subscripts 1 and 2 refer to the pure liquid and dry polymer, respectively; and $n(X')$ and ℓ_X denote the refractive index and the thickness of the swollen polymer at X', respectively. Under conditions where the swelling polymer is constrained to a uniform

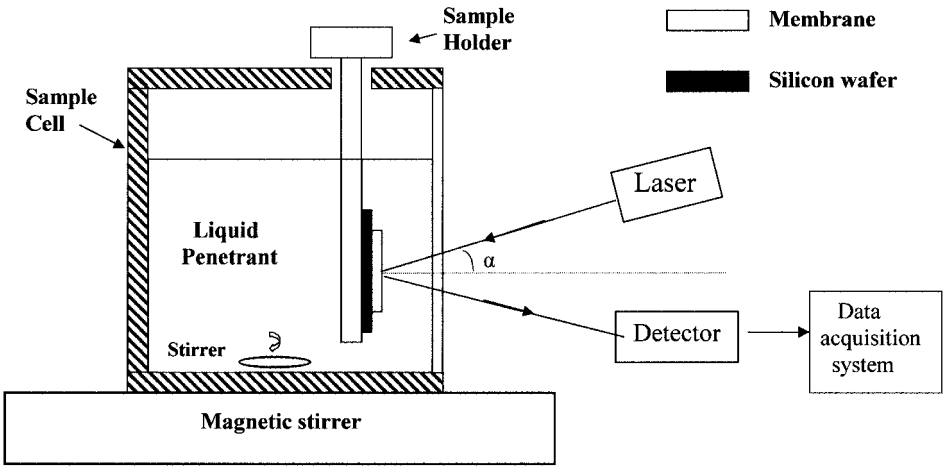

Figure 2 Schematic presentation of experimental setup for laser interferometry measurements during liquid penetration in very thin supported PMMA films.

thickness (i.e., $\ell_X = \ell_1 = \ell_2$), and in the absence of significant changes of volume upon mixing, the OPD profile is expected to faithfully represent the corresponding concentration profile.[12,13,29]

The microscope (as well as the laser interferometer described below) was situated in a small room equipped with two air-conditioning devices, capable of maintaining its temperature at 22 ± 1°C. This was ensured by recording the temperature before each measurement. Experiments during which the temperature exceeded the above range were discarded. All penetration kinetic and OPD experiments were repeated in at least three polymer samples.

Laser Interferometry

In the current work an experimental laser interferometer tool was used with high data acquisition capability.[30] The supported PMMA film, properly mounted on a holder, resided in a glass cell equipped with a quartz window and filled with the liquid penetrant (Fig. 2). During all the experiments the liquid penetrant was stirred with a magnetic stirrer. A laser beam emitting at $\lambda = 638$ nm (at this wavelength the absorption in the film is negligible) was directed, at near-normal incidence, to the polymer–solution interface. Part of the light beam was reflected from this interface. The rest traveled in the polymer film and, because of the refractive index difference between the polymer film and the silicon substrate, was reflected from the polymer–substrate interface. The reflected beams fell on a detector and the measured intensity varied with time during sorption experiments as a result of thin film interference effects. In the simple case of one distinct polymer–liquid interface moving at constant velocity throughout the film, an oscillatory signal of constant period and amplitude was obtained. The thickness change $d\ell$ of the dissolving polymer, corresponding to the period of oscillation, is given by

$$d\ell = \frac{\lambda}{2\sqrt{n_2^2 - n_1 \sin^2\alpha}} \tag{3}$$

where α is the angle of beam incidence.

Before each experiment, a blank sample (silicon wafer without a polymer film) was aligned in the cell, the cell was filled with the penetrant, and the baseline output was recorded. The data acquisition was properly initiated with the sample insertion and the intensity recorded with a rate higher than 100 measurements/s.

RESULTS AND DISCUSSION

Optical Microscopy and Two-Beam Interferometry on Clamped Films

Solvent Penetrants

Dissolution of PMMA by pure MEK was accompanied by stress cracking. Shortly after immersion of the polymer film in the pure liquid penetrant, front B developed a sawtoothlike appearance, as shown in Figure 3(a), indicative of microcrack formation, and small irregular frag-

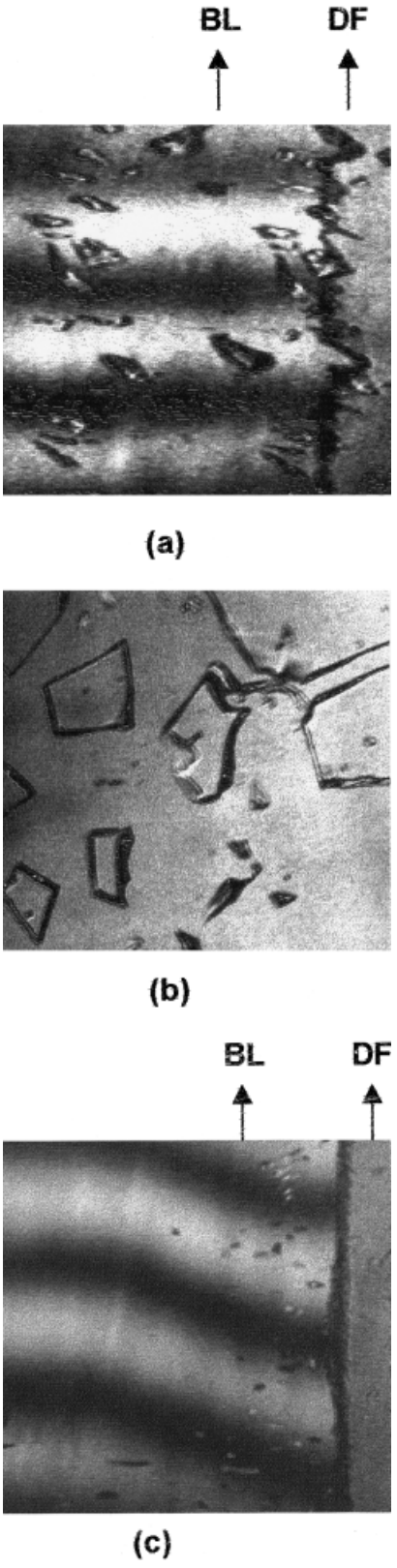

Figure 3 Photographs taken during dissolution of clamped PMMA films. (a) Interference fringe pattern taken during the initial stages of dissolution by pure MEK. BL, bulk liquid; DP, dry polymer film. The fringes in the dry polymer film are outside the optical field covered by this photograph. (b) Final stages of intense fragmentation during dissolution by pure MEK. (c) Interference fringe pattern taken during the initial stages of dissolution by 80 : 20 v/v MEK/MA. Notation as in (a).

ments of polymer were detached from the bulk polymer. The fringe pattern in the pure liquid phase remained undisturbed up to front B, indicating the absence of any surface layer behind front B during dissolution. Eventually the microcracks of Figure 3(a) developed into more sizable cracks, which advanced in random directions into the dry polymer and crossed, thus causing intense fragmentation of the polymer [Fig. 3(b)]. Solvent-induced cracking of PMMA was previously reported in many cases, that is, during dissolution by MEK,[8,27,31] acetone,[27] MIBK,[31] tetrahydrofuran,[31] methyl acetate,[7] and isopropyl alcohol/MEK mixtures,[11] and has been attributed to solvent-induced osmotic stresses, which cause brittle failure at weak points of the sample's structure. For a particular polymer, the occurrence and initiation time for crack development depend on the solvent's swelling power, prior thermal and mechanical history of the polymer sample, initial conditions imposed on the experiments, and the polymer sample's geometry.[31]

In the present work, during the period preceding intense fragmentation of the polymer film, the propagation of front B could be measured and, as shown in Figure 4, followed Case II kinetics. The mean penetration rate dX_B/dt was found to be 0.36 ± 0.08 μm/min, within the range of 0.16–0.4 μm/min of dissolution rates found by other investigators for the same system.[10,15,16,27,28] The corresponding OPD profile (Fig. 5) indicates the existence of a penetrant precursor front (consisting of the infiltration and solid layers, according to Ueberreiter's[7] terminology) ahead of front B. This narrow precursor front in conjunction with the serrated B front indicate that initial penetration of MEK into the unrelaxed dry polymer is slow and uneven (mostly into lower-density areas) and substantial swelling occurs by brittle failure with a high τ_R. Case II penetration kinetics indicate that once swelling occurs, diffusion through the swollen layer is very rapid, leading to a high MEK concentration at X_B. The vanishing thickness of the surface layer should be attributed to very small N_s, consistent with the high solvent power of MEK and the high MEK concentration at X_B.

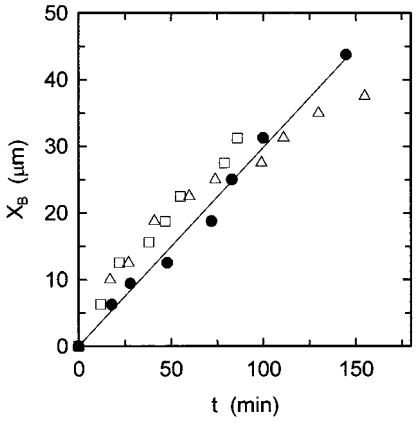

Figure 4 Representative kinetic data of front B penetration during dissolution of clamped PMMA films by: pure MEK (●); 80 : 20 v/v MEK/MA (□); 50 : 50 v/v MEK/MA (△).

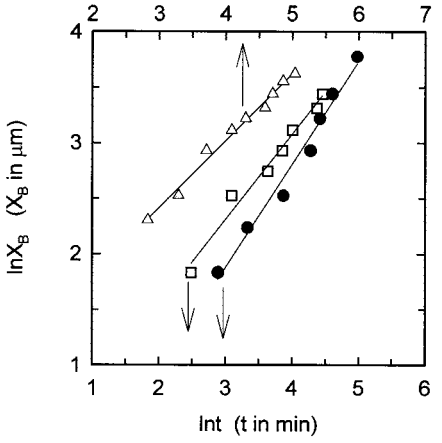

Figure 6 Data of Figure 4 replotted here on a double logarithmic scale. Values of exponent of eq. (1) deduced from the respective slopes: $m = 0.99$ (pure MEK, ●); $m = 0.76$ (80 : 20 v/v MEK/MA, □); $m = 0.60$ (50 : 50 v/v MEK/MA, △).

Mixtures of 80 : 20, 60 : 40, and 50 : 50 v/v MEK/MA also dissolved PMMA. Representative data of the propagation kinetics of front B for the 80 : 20 and 50 : 50 v/v MEK/MA mixtures are included in Figure 4. The corresponding OPD profiles for all solvent compositions are included in Figure 5, and the fringe pattern for the 80 : 20 MEK/MA mixture is shown in Figure 3(c). The main features of the dissolution by MEK/MA mixtures are as follows:

1. As in the case of pure MEK, the OPD profiles exhibit a penetrant precursor front ahead of front B. Although it is difficult to establish the exact shape of this precursor front, its width clearly tends to increase with increasing MA content of the penetrant mixture (Fig. 5).
2. In contrast to dissolution by pure MEK, the OPD profiles of the mixtures exhibit definite gradients behind front B [Figs. 3(c) and (5)], indicating the existence of a surface layer of low polymer concentration, which was found to attain a constant thickness within the experimental time of observation. The OPD gradients tend to become more pronounced with rising MA content of the mixture.
3. The onset of fragmentation was delayed and its intensity reduced when the MA content of the mixture was increased, until finally no discernible crack formation occurred in the case of the 50 : 50 mixture.
4. Increasing deviations from pure Case II kinetics were observed with rising MA content in the mixture. This can be clearly seen by plotting the data of Figure 4 on a log–log scale, as shown in Figure 6. The relevant plots conform to eq. (1) reasonably well; the corresponding mean values of m, deduced from log–log plots, were $m = 0.95 \pm 0.03$ for pure MEK, $m = 0.78 \pm 0.07$ for 80 : 20, and $m = 0.60 \pm 0.01$ for the 50 : 50 MEK/MA mixture.
5. The mean rates of penetration (deduced from the initially linear part of the X_B versus t curves of the type shown in Fig. 4) plotted as a function of MEK content of the penetrant mixture in Figure 7, show an en-

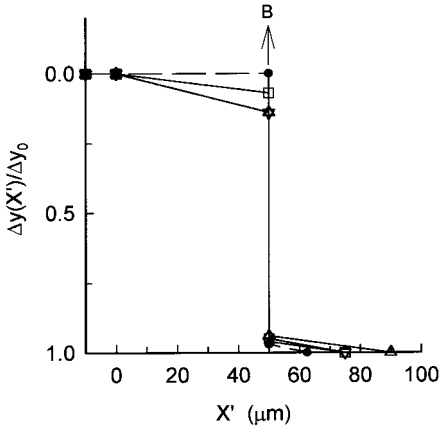

Figure 5 Representative optical path difference profiles $\Delta y(X')/\Delta y_0$ obtained during dissolution of clamped PMMA films by: pure MEK (●); 80 : 20 v/v MEK/MA (□); 60 : 40 v/v MEK/MA (▽); 50 : 50 v/v MEK/MA (△).

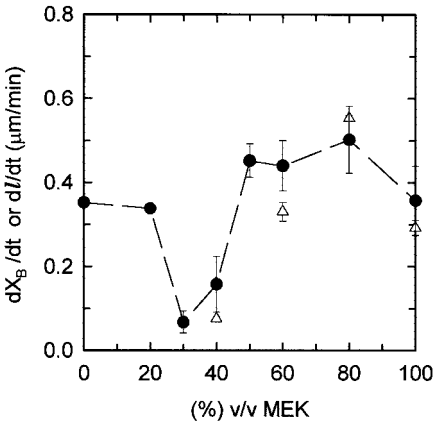

Figure 7 Penetration rate dX_B/dt deduced from optical microscopy experiments on clamped PMMA films (●) and dissolution rate $d\ell/dt$ deduced from laser interferometry experiments on thin supported PMMA films (△), versus the composition of the MEK/MA liquid mixture.

hancement of penetration (and dissolution) rate at intermediate compositions of MEK/MA mixtures. A similar effect has been observed during dissolution of PMMA by MIBK/MA[28] and MEK/water[22] mixtures.

The above features constitute a complex but informative picture of the effect of MA composition on the dissolution mechanism of PMMA by MEK/MA mixtures, which can be interpreted in a qualitative but consistent manner.

We first note that, although sorption of MEK in PMMA is thermodynamically favored, feature (1) clearly indicates that MA, thanks to its smaller molecular size, infiltrates the dry polymer more extensively than MEK. As a result of the consequent plasticization effect, the polymer becomes less brittle and cracking is prevented to some extent (feature 3). MA-induced plasticization also facilitates swelling deformability, thus increasing the rate of relaxation (lower τ_R). As a result of decreased τ_R, diffusion of the penetrant to front B occurs at time scales comparable to those of the relaxation process at the front, and penetration becomes partly diffusion-controlled, as evidenced by the observed deviations from Case II kinetics (feature 4). On the other hand, in the thermodynamically less favorable environment of MEK/MA mixtures, compared to that of pure MEK, the disentanglement of the polymer chains and their further diffusion toward the pure penetrant phase are expected to be hindered compared to that of pure MEK (higher τ_d). Thus these processes occur at finite times compared to the time of relaxation at front B, and a surface layer of low and gradually decreasing polymer concentration is formed behind front B (feature 2). Finally, the enhancement of penetration rate at the initial stages of penetration of MEK/MA mixtures, compared to the penetration of pure MEK (feature 5), should be attributed to the lower relaxation time τ_R prevailing in the former cases.

The above discussion indicates that MEK/MA mixtures are thermodynamically poorer but kinetically better solvents of PMMA compared to pure MEK. Thus, in terms of DEB number, penetration of MEK/MA mixtures is characterized by lower DEB number values (resulting in deviations from Case II kinetics), compared to that of pure MEK, because of lower relaxation times τ_R (resulting in initially enhanced relaxation-controlled penetration rates). In terms of N_s numbers, dissolution of the said mixtures is characterized by higher N_s values (attributed to an increase of τ_d and a concurrent decrease of τ_R) compared to that of pure MEK.

Nonsolvent Penetrants

The OPD profile obtained during transport of pure MA in PMMA is presented in Figure 8. The low sorptive capacity of PMMA in pure MA is evidenced by the large discontinuity at the swollen polymer–pure MA interface, which gives rise

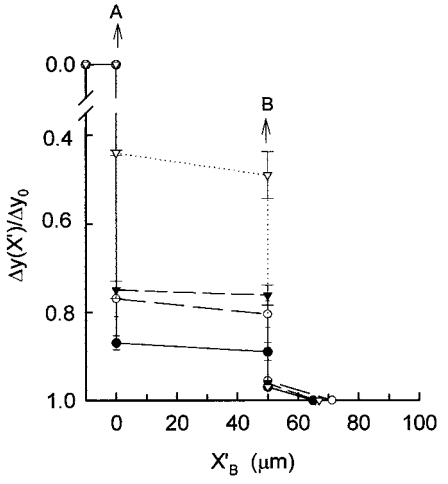

Figure 8 Representative optical path difference profiles $\Delta y(X')/\Delta y_0$ obtained during penetration of nonsolvents in clamped PMMA films: pure MA (●); 20 : 80 v/v MEK/MA (○); 30 : 70 v/v MEK/MA (▼); 40 : 60 v/v MEK/MA (▽).

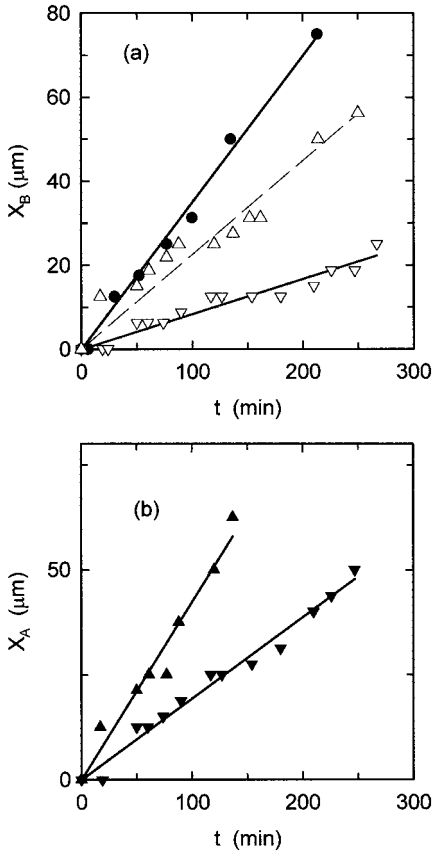

Figure 9 Representative kinetic data for transport of nonsolvents in clamped PMMA films. (a) Penetration front B: pure MA (●); 30 : 70 v/v MEK/MA (▽); 40 : 60 v/v MEK/MA (△). (b) Swelling front A: 30 : 70 v/v MEK/MA (▼); 40 : 60 v/v MEK/MA (▲).

to the visible swelling front A. A less-dramatic but still relatively sharp rise of $\Delta y(X')/\Delta y_0$ (representing a corresponding drop of MA concentration) is observed near the dry polymer region, giving rise to the visible penetrant front B. The OPD profile between fronts A and B is flat, and a low MA precursor front is observed ahead of B. The propagation of front B was found to be linear with time [Fig. 9(a)], whereas the movement of front A was scarcely discernible. Thus, in line with previous findings,[14,21] penetration of pure MA exhibits all the essential characteristics of Case II transport described earlier in the introductory section. The rate dX_B/dt was found to be 0.35 ± 0.01 μm/min, within the range 0.1–0.40 μm/min reported previously[14,21] for the same system.

Addition of 20% v/v MEK in the liquid penetrant did not have any appreciable effect on the kinetics and the rate of front B propagation. The shape of the OPD profile remained essentially the same (Fig. 8). The lower $\Delta y(X')/\Delta y_0$ values in the region $0 \leq X' \leq X'_B$, compared to values for penetration of pure MA, indicate an enhancement of the overall level of sorption attributed to the presence of MEK in the liquid penetrant mixture. For the 30 : 70 MEK/MA mixture, the OPD profile (Fig. 8) is very similar in shape, as well as in numerical values of $\Delta y(X')/\Delta y_0$ with the OPD profile for the 20 : 80 MEK/MA mixture, indicating that sorption in the swollen polymer did not drastically change. On the other hand, the rate of front B propagation is reduced [Fig. 9(a)], whereas the movement of front A becomes measurable [Fig. 9(b)]. A further increase of the MEK content of the liquid penetrant mixture to 40 : 60 MEK/MA composition resulted in increased sorption levels in the polymer (as shown by the corresponding OPD profile in Fig. 8) and increased rates of propagation of both fronts A and B [Figs. 9(a) and 9(b), respectively]. For all nonsolvent mixtures studied, the movement of both fronts conformed reasonably well to Case II kinetics, and mean values of the corresponding rates dX_B/dt are included in Figure 7. In line with the absence of any significant diffusion limitations in the relaxation-controlled propagation of front B, the corresponding OPD profiles were more or less flat in the $0 \leq X' \leq X'_B$ region.

A possible interpretation of the observed minimum in the rate of front B at low MEK compositions can be based on the assumption that the presence of small amounts of sorbed MEK in the swelling polymer does not significantly contribute to the penetration at front B, because of its low activity and the restrictions imposed in penetration by its relatively larger molecular size compared to that of MA. Its main effect is to reduce the driving force for MA penetration, through the reduction of MA's activity in the liquid mixture. This reduction seems to have no discernible effect on the rate of penetration for the 20 : 80 MEK/MA mixture, but becomes significant for the 30 : 70 MEK/MA composition, and as a result the penetration rate of front B is reduced [Fig. 9(a)]. On the other hand, because of the thermodynamic compatability of MEK with PMMA, even small amounts of MEK induce significant plasticization of the penetrated region of polymer, which can now more easily swell in the $-X$ direction [Fig. 9(b)]. Upon further increasing the MEK content to 40 : 60 MEK/MA composition, a considerably higher level of sorption is attained in the polymer, as evidenced by the OPD profile, and the threshold for dissolution is approached. Because of the

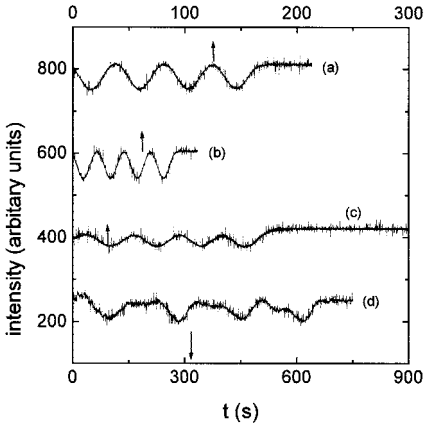

Figure 10 Interferometric signal during exposure of supported PMMA film to (a) pure MEK; (b) 80 : 20 v/v MEK/MA; (c) 60 : 40 v/v MEK/MA; (d) 40 : 60 MEK/MA mixtures.

contribution of MEK in the penetration rate, as a result of its increased activity in the mixture, the rate of front B is increased [Fig. 9(a)]. Also, as a result of higher sorption and consequent intense plasticization effects, the rate of front A is also increased [Fig. 9(b)].

Laser Interferometry on Thin Supported Films

The interferometric signal obtained during exposure of a supported 0.9-μm-thick PMMA film in pure MEK is shown in Figure 10. The sinusoidal signal, consisting of one oscillatory component with constant amplitude and period, indicates the existence of one distinct polymer–liquid interface moving at constant velocity throughout the film,[22] in line with the results of optical microscopy and two-beam interferometry. The period of oscillation, measured from peak to peak, in conjunction with eq. (3) yields a rate of thickness change $d\ell/dt = 0.29 \pm 0.02$ μm/min, very close to the mean rate of penetration dX_B/dt obtained from optical microscopy.

The interferometric signals for the 80 : 20 and the 60 : 40 MEK/MA mixtures (also shown in Fig. 10) depict essentially the same features as the signal for pure MEK, except for the fact that, in the case of the 60 : 40 mixture, the maxima of the interferometer trace are lower in intensity compared with that of the final baseline, produced from the reflection on the bare substrate. This feature points to a reduction of the sharpness of the penetrant front,[15,24] possibly attributable to a surface layer and/or an extended precursor front (Fig. 5). The constant period of oscillation for both mixtures indicates the absence of deviations from Case II transport during the laser interferometry experiments, in contrast to the results of optical microscopy (Figs. 4 and 6). This is expected, given that the maximum penetration distances in the former experiments are about 1 micron, and thus correspond to the initially linear (Case II) part of the X_B versus t plots of Figure 4. The main point of interest here is that the rates $d\ell/dt$ deduced from the laser interferometry experiments and included in Figure 7, show the same trend, as well as similar numerical values, with increasing MEK content as the corresponding results of front B initial penetration rate dX_B/dt.

We also applied laser interferometry in the 40 : 60 MEK/MA mixture. The results, shown in Figure 10, depict two partially superimposed oscillatory components, in line with the existence of two distinct interfaces (fronts A and B) found in the optical microscopy and two-beam interferometry experiments. Although it is not possible to obtain reliable rates from this signal, we may note that the time needed for completion of the process is considerably longer than the corresponding times of the solvent mixtures of higher MEK content. In fact, by dividing the initial thickness (0.9 μm) of the sample by the time needed for completion of the process (650 s), a rate of 0.08 μm/min is obtained, within the limits of experimental error of the penetration rate dX_B/dt ($=0.15 \pm 0.06$ μm/min) deduced from optical microscopy experiments.

CONCLUSIONS

In the present work we report the swelling and dissolution behavior of PMMA films during unidimensional penetration of MEK/MA mixtures at 22°C. Optical microscopy and two-beam interferometry with a light beam perpendicular to the axis of penetration were applied to clamped PMMA films, to study the full range of compositions of solvent–nonsolvent mixtures. Laser interferometry with a light beam parallel to the direction of penetration was applied to very thin PMMA films, supported on a silicon substrate, to study selected cases.

The main findings by application of the former techniques are as follows:

1. The transition from dissolution to swelling behavior occurred in the region between 50 :

50 and 40 : 60 v/v MEK/MA compositions, very similar to the corresponding transition region found previously for MEK/isopropyl alcohol and MIBK/MA mixtures at 24.8°C.[27]

2. Dissolution by pure MEK was controlled by Case II penetration kinetics. Swelling at the penetration front (B) generated brittle failure, which eventually led to fragmentation. The vanishing thickness of the surface layer behind front B indicates that dissolution was characterized by low N_s number as a result of the high relaxation time τ_R at the front and the low chain disentanglement time τ_d, consistent with the high solvent power of MEK.
3. Introduction of MA in the liquid solvent resulted in a more efficient penetration of the smaller MA molecules into the dry unrelaxed polymer, as evidenced by the more prominent precursor fronts ahead of front B. As a result of MA-induced plasticization, fragmentation was delayed compared to that in pure MEK and the time τ_R of the relaxation process at the front was reduced, as evidenced by the enhanced penetration rates at the early stages of the process. The observed deviations from Case II kinetics at the later stages are also attributed to a lower τ_R, resulting in partly diffusion-controlled kinetics. The existence of a surface layer behind front B indicates that dissolution by MEK/MA mixtures is characterized by higher N_s numbers attributed to the decrease of τ_R and a concurrent increase of τ_d, consistent with the lower solvent power of the said mixtures compared to that of pure MEK.
4. Swelling by pure MA, as well as by nonsolvent MEK/MA mixtures, was characterized by Case II kinetics of penetration and by small concentration gradients in the swollen polymer region between the swelling edge A of the film and the advancing penetrant front B. The extent of absorption was found to be low for MA and increased with increasing MEK content. In line with the resulting increased plasticization of the penetrated polymer, the rate of swelling front A was also found to increase with increasing MEK content. On the other hand, a pronounced minimum in the penetration rate versus mixture composition was observed at 30 : 70 MEK/MA. A possible interpretation may be based on the assumption that the larger MEK molecules in the penetrant mixture reduce the driving force for MA penetration, without effectively contributing to penetration at the front itself.

The main features of the laser interferometric signal for pure MEK, as well as for the 80 : 20 and 60 : 40 MEK/MA mixtures, indicated the existence of one distinct front moving linearly with time, in line with the results obtained by optical microscopy. In addition, the deduced rates of dissolution showed the same trend with increasing MA content as that of the experiments in clamped PMMA films. The signal for the 40 : 60 MEK/MA was consistent with the existence of two moving sharp fronts, in line with the results in clamped films.

The laser interferometry technique applied in thin supported films is a simple and fast method for the evaluation of the lithographic characteristics of a certain polymer-developer system. On the other hand, reliable conclusions are easily reached only for Case II dissolution rate in the absence of a surface layer that reduces the sharpness (and thus the reflectivity) of the sharp front. Otherwise, either a solvent concentration profile has to be adopted *a priori* to interpret the interferometric signal, or another experimental technique, yielding additional information on the transport process, has to be applied.[24] The techniques of optical microscopy and two-beam interferometry applied in this study require considerably thicker films, pressed between glass plates to ensure penetration along the plane of the film. Thus both the direction of penetration into the film and the external constraints imposed on its swelling differ from those prevailing in the laser interferometric technique, which corresponds more closely to the conditions of lithography. In spite of these differences, the results obtained here by these techniques are very similar (not only with respect to the transport and dissolution mode, but also with respect to the numerical values of rates of penetration and dissolution). This finding is very promising in the sense that the aforementioned techniques can be used jointly to gain further insight into the phenomena of interest in lithography, bearing in mind that two-beam interferometry can provide reliable information on the penetrant concentration profile independently of the nature of the kinetics of penetration.

This work was supported by internal Grant No. 602 in the framework of the "Demoerevna" Program of the National Research Center Demokritos.

REFERENCES

1. Thomas, N. L.; Windle, A. H. Polymer 1982, 23, 529.
2. Petropoulos, J. H. J Polym Sci Polym Phys Ed 1984, 22, 1885.
3. Durning, C. J. J Polym Sci Polym Phys Ed 1985, 23, 1831.
4. Wu, J. C.; Peppas, N. A. J Polym Sci Part B: Polym Phys 1993, 31, 1503.
5. Vrentas, J. S.; Jarzebski, C. M.; Duda, J. L. AIChE J 1975, 21, 894.
6. Petropoulos, J. H. J Polym Sci Polym Phys Ed 1984, 22, 183.
7. Ueberreiter, K. in Diffusion in Polymers; Crank, J.; Park, G. S., Eds.; Academic Press: New York, 1968; Chapter 7.
8. Peppas, N. A.; Wu, J. C.; von Meerwall, E. D. Macromolecules 1994, 27, 5626.
9. Rai-Choudhury, P., Ed. Handbook of Microlithography, Micromachining and Microfabrication; SPIE Optical Engineering Press: Bellingham, WA/IEE: London, 1997.
10. Limm, W.; Winnik, M. A.; Smith, B. A.; Stanton, D. T. Polymers in Microlithography; ACS Symposium Series 23; American Chemical Society: Washington, DC, 1989; p 385.
11. Pethrick, R. A.; Rankin, K. E. J Mater Chem 1998, 8, 2591.
12. Sanopoulou, M.; Petropoulos, J. H. J Polym Sci Part B: Polym Phys 1992, 30, 971.
13. Stamatialis, D. F.; Sanopoulou, M.; Petropoulos, J. H. J Polym Sci Part B: Polym Phys 1997, 35, 2593.
14. Durning, C. J.; Hassan, M. M.; Tong, H. M.; Lee, K. W. Macromolecules 1995, 28, 4234.
15. Krasicky, P. D.; Groele, R. J.; Jubinsky, J. A.; Rogriguez, F. Polym Eng Sci 1987, 27, 282.
16. Zhu, X. X.; Wang, F.; Nivaggioli, T.; Winnik, M. A.; Macdonald, P. M. Macromolecules 1993, 26, 6397.
17. Papanu, J. S.; Hess, D. W.; Bell, A. T.; Soane, D. S. J Electrochem Soc 1989, 136, 1195.
18. Papanu, J. S.; Hess, D. W.; Soane (Soong), D. S.; Bell, A. T. J Appl Polym Sci 1990, 39, 803.
19. Narasimhan, B.; Snaar, J. E. M.; Bowtell, R. W.; Morgan, S.; Melia, C. D.; Peppas, N. A. Macromolecules 1999, 32, 704.
20. Mills, P. J.; Palmstrom, C. J.; Kramer, E. J. J Mater Sci 1986, 21, 1479.
21. Thomas, N.; Windle, A. H. Polymer 1978, 19, 255.
22. Rodriguez, F.; Krasicky, P. D.; Groele, R. J. Solid State Technol 1985, 28, 125.
23. Pethrick, R. A.; Rankin, K. E. J Mater Chem 1998, 8, 2599.
24. Limm, W.; Stanton, D.; Dimnik, G. P.; Winnik, M. A.; Smith, B. A. J Appl Polym Sci 1988, 35, 2099.
25. Pekcan; O.; Ugur, S.; Yilmaz, Y. Polymer 1997, 38, 2183.
26. Pekcan, O.; Canpolat, M.; Kaya, D. J Appl Polym Sci 1996, 60, 2105.
27. Papanu, J. S.; Hess, D. W.; Soane, D. S.; Bell, A. T. J Electrochem Soc 1989, 136, 3077.
28. Manjikow, J.; Papanu, J. S.; Soong, D. S.; Hess, D. W.; Bell, A. T. J Appl Phys 1987, 62, 682.
29. Stamatialis, D. F.; Sanopoulou, M.; Petropoulos, J. H. J Appl Polym Sci 1997, 65, 317.
30. Raptis, I. Presented at the Micro and Nano Engineering Conference, Jena, Germany, September 2000; Paper No. 000.
31. Ouano, A. C.; Carothers, J. A. Polym Eng Sci 1980, 20, 160.